CHS T-JOINTS STRENGTHENED WITH EXTERNAL STIFFENERS UNDER BRACE AXIAL TENSION

YUNAN DING[1], LEI ZHU[2]*, YU BAI[3], HAILINSUN[4]

[1]*School of Civil and Transportation Engineering, Beijing University of Civil Engineering and Architecture, Beijing, China*
[2]*School of Civil and Transportation Engineering, Beijing University of Civil Engineering and Architecture, Beijing, China*
[3]*Department of Civil Engineering, Monash University, Clayton, Australia*
[4]*China Architecture Design and Research Group, Beijing, China*
E-mail: zhulei@bucea.edu.cn

This study reports a series of experimental and numerical investigations of circular hollow section (CHS) T-joints strengthened by external stiffeners. Six full-scale specimens divided into three groups were tested, including three brace to chord diameter ratios of 0.25, 0.50, and 0.73. The detailed parameters of specimens as well as the experimental devices are presented, meanwhile the test results including failure modes, load-displacement curves are analysed and compared. Compared with unreinforced specimens, the reinforced specimens show a significant enhancement in joint capacity in tension, with an increase of about 14% to 33% for ultimate strength and up to about 30% respectively for initial stiffness in comparison to unreinforced specimens. SHELL181 element is used to build finite element modeling which accurately predicts the structural performance of six T-joints, including deformed shape and ultimate strength.

Keywords: Circular hollow section, T-joint, Axial tension, External stiffener, Full-scale testing, Finite element modeling.

1 Introduction

The use of circular hollow section (CHS) tubular structures is becoming increasingly popular over past decades. Nowadays, CHS tubular structures are used in diverse buildings, such as airports, railway stations, bridges and long-span roofs (Luo et al. 2016, Yang et al. 2016, Yang et al. 2017). In these structures, the connection is the most important part and there are many methods to improve the mechanical properties of the joints.

However, most previous studies have focused on compression behavior, with very limited research into the ultimate strength of reinforced T-joints under axial tension. Choo et al. (2005) and van der Vegte et al. (2005) investigated the mechanical behavior of CHS T-joints strengthened by collar and doubler plates through experimental studies and numerical simulations. The static test results indicated obvious strength enhancement. Such collar and doubler plate reinforcements were further studied by Feng and Tan (2005), Hossein et al. (2016), and Sui et al. (2013). Wang et al. (2014) presented calculation equations for the bearing capacity of internal ring-stiffened joints. Six full-scale CHS X-joints were tested under tensile stress in order to investigate the mechanical performance (Ding et al. 2018).

Proceedings of the 17th International Symposium on Tubular Structures.
Editors: X.D. Qian and Y.S. Choo
Copyright © ISTS2019 Editors. All rights reserved.
Published by Research Publishing, Singapore.
ISBN: 978-981-11-0745-0; doi:10.3850/978-981-11-0745-0_059-cd

In view of the lack of relevant research work for the reinforced T-joints in axial tension, this paper focuses on the behavior of external stiffener strengthening CHS T-joints subjected to brace axial tensile load. The specimens tested in the experiment covered three different values (0.25, 0.50, and 0.73) of the brace to chord diameter ratio. In addition, the chord deformation, failure modes and ultimate strength were carefully recorded. Furthermore, finite element (FE) models were built to simulate the whole loading process of joints and the accuracy of it was verified by experimental results.

2 Experiment Program

2.1 *Test setup*

The experimental device of T-joints is shown in Fig. 1. The specimen was fixed at the brace end and each chord end was subjected to a vertical upward force from a 100-ton actuator acting directly on the end plate to replicate brace axial tension. The distance of the load points of the two actuators was 2300mm (Fig. 1). The brace end was fixed to the ground. Each specimen was loaded by displacement-controlled method, and two loading rates were used during experiment. Specifically, in linear load range, the initial rate was 1.0mm/min for the linear load range and then declined to 0.3mm/min at elastic-plastic load range.

The boundary condition of the specimen was equivalent to the simply supported condition and no chord axial load was produced during the experiment. As shown in Fig. 1, a linear variable displacement transducer (LVDT1) was placed on the mid-span of the chord to measure the chord ovalization. LVDT2 and LVDT3 were placed at the brace end plate and one transducer (LVDT4 and LVDT5) was placed at each chord end, monitoring the vertical displacement between chord and brace end.

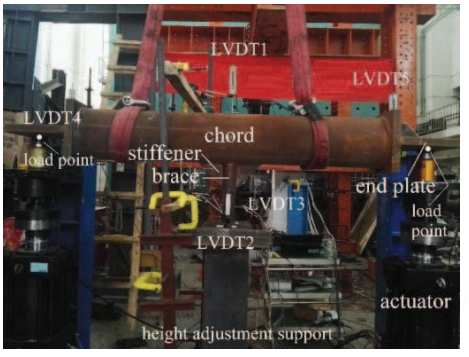

Figure 1. Experiment setup

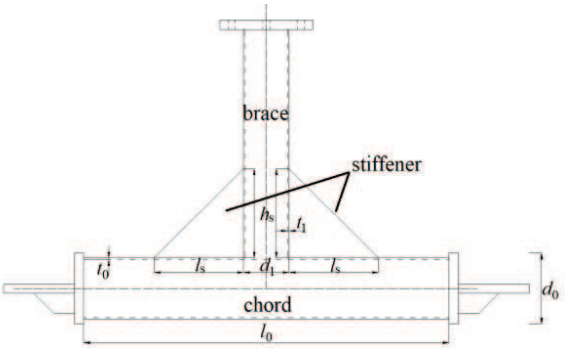

Figure 2. Schematic arrangement of specimens

2.2 *Specimen geometry and material properties*

Fig. 2 shows the geometrical parameters of T-joint specimens. Generally, a complete definition of a T-joint strengthened by external stiffeners includes the following parameters: the chord diameter (d_0), the brace diameter (d_1), chord length (l_0), brace length (l_1), chord wall thickness (t_0), brace wall thickness (t_1), the stiffener thickness (t_s), the stiffener length (l_s) and height (h_s), chord length to radius (α), brace to chord diameter (β), chord diameter to double chord wall thickness (γ), and brace wall thickness over chord wall thickness radio (τ). For each joint, l_s and h_s were double d_1 meanwhile t_s was 8mm. One steel plate of 45 mm thickness which had bolt boles was welded on the top of the brace, and two 45 mm thickness end plates with stiffeners were welded at chord ends. The specific parameters are shown in Table 1.

Table 1. Specimen parameters

Specimen	Type	d_0(mm)	d_1(mm)	t_0(mm)	t_1(mm)	l_1(mm)	β	γ	τ
T-025	unreinforced	300.0	76.0	8.10	6.10	368.5	0.25	18.52	0.75
T-025-R	reinforced	300.0	76.0	7.86	5.92	375.6	0.25	19.08	0.75
T-050	unreinforced	300.0	151.0	8.34	8.59	745.6	0.50	17.99	1.03
T-050-R	reinforced	300.0	151.0	8.18	8.52	746.5	0.50	18.34	1.04
T-073	unreinforced	300.0	219.0	8.10	8.15	1122.5	0.73	18.52	1.01
T-073-R	reinforced	300.0	219.0	8.12	8.33	1123.6	0.73	18.47	1.03

All the CHS tubes used to fabricate joints were hot-rolling seamless and low carbon steel tubes. To ensure the consistency of material properties, all six chords were taken from one tube. The chord was welded with the brace using the fillet weld and the weld size was determined in accordance with Eurocode 3 recommendations (2016), and the throat thickness was 11mm. Three coupons were cut from each of the steel plate, which was used to make chord, brace and stiffener members. Young's modulus and yield stress for each component were determined by coupon tests, according to the Chinese standard (2010). The Young's modulus of the chords and stiffeners were 193.7GPa and 246.5GPa, the yield stress were 284.7MPa and 358.3MPa. For the braces that β=0.25, 0.50 and 0.73, their Young's modulus were 222.3GPa, 240.0GPa and 244.3GPa, their yield stress were 313.3MPa, 295.0MPa and 317.7MPa.

3 Experimental results

In order to define the ultimate strength in these circumstances, the deformation limit is defined as 6%d_0 relative to the chord bottom line as in Choo et al. (2005) and van der Vegte et al. (2005) or as 3%d_0 relative to the chord centre line recommended by Lu et al. (1994).

3.1. *Failure modes*

After each specimen was tested, a section or ring segment was cut from the mid-span of the chord by flame-cutting. The deformations at brace-chord intersection regions could be seen clearly through these sections, as shown in Fig. 3 (left). (Fig. 3 (right) is explained in section 4, FE modeling) The test was stopped when cracking occurring at the welding line near the saddle position of the chords for T-025 specimen, as shown in Fig. 4.

Fig. 5 shows the deformed configuration of T-050-R after the brace tension test, and this deformation characteristic is a typical representative of all tested specimens except T-025. As shown in Fig. 3 and Fig. 5, the dominant deformation of these specimens is overall bending deformation of the chord, together with macroscopic but not remarkable chord ovalization at mid-span. The tests were stopped when significant vertical deformation (the displacement between brace and chord end reached 45 mm) occurred at the joint.

In general, the deformation characteristics can be classified into two types. On the one hand, the hot spot lies very close to the saddle area for axially loaded T-joints and therefore the crack occurs at the saddle point. On the other hand, the main deformation of the joints is in the form of the chord bending deflection, increasing with the β value. In T-025, the weld crack occurred before the chord ovalization reached 6%d_0. In T-025-R, T-050 and T-050-R, the 6%d_0 chord ovalization criterion was achieved during the process of chord bending deformation. However, in T-073 and T-073-R, no sufficient chord ovalization appeared throughout the experiment and the main deformation was chord bending. Hence, the failure mode in T-025 was weld failure, in T-025-R, T-050 and T-050-R it was chord plastification, and no joint failure occurred in specimens T-073 and T-073-R.

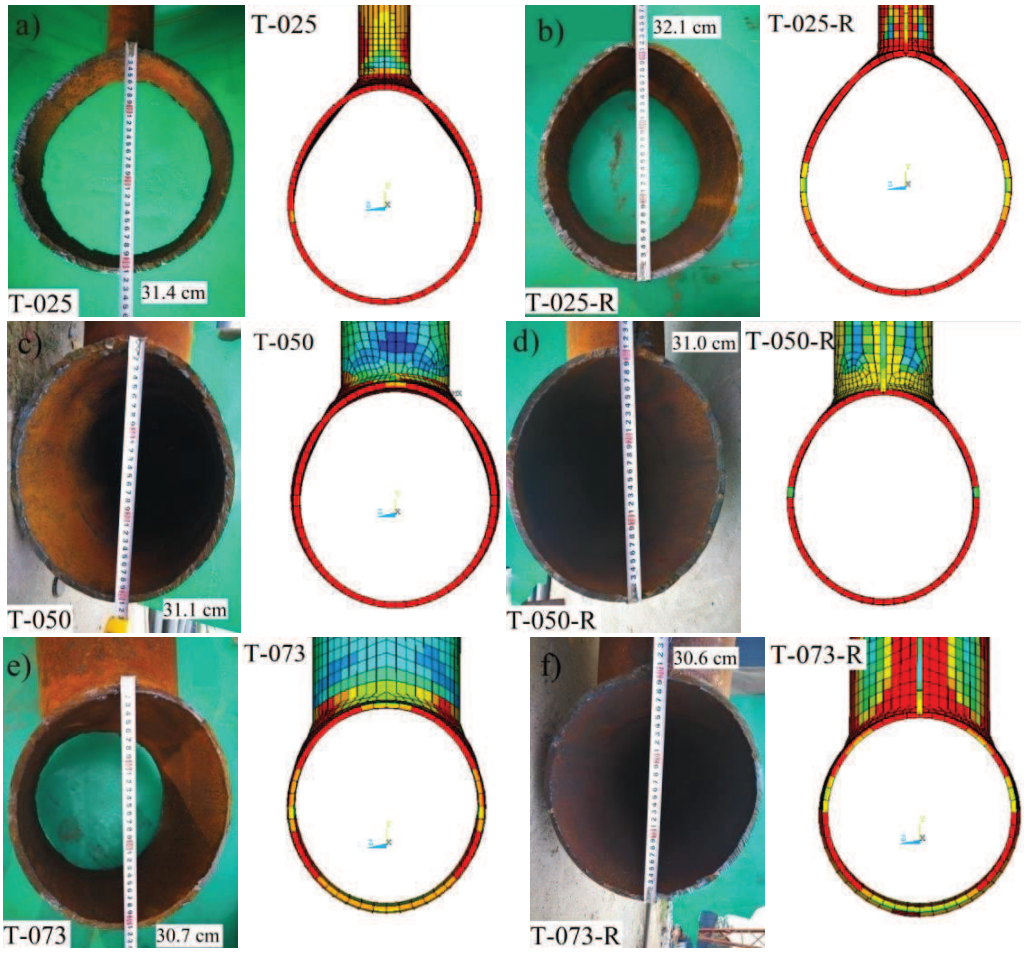

Figure 3. Deformed shapes of specimens after loading

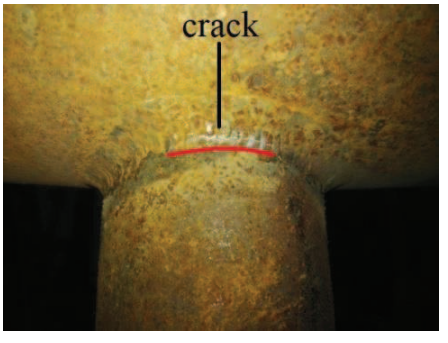

Figure 4. Weld crack of specimen T-025

Figure 5. Deformation of specimen T-050-R

3.2. *Load-ovalization curves*

The load-ovalization curves of specimens T-025, T-025-R, T-050 and T-050-R are shown in Fig. 6 a), where the ovalization is the value recorded by LVDT1 fixed at the chord mid-span. It is shown that the curves exhibit a continuous trend of increase in load with ovalization. For T-025, the curve reaches its peak when the weld failure appears at the weld region.

For specimens T-073 and T-073-R, the load-ovalization experimental data were lost due to the breakdown of data recording instrument. However, the load-ovalization curve which is calculated by the FE analysis can be used as the auxiliary method to determine the ultimate strength of these two specimens after confirming the validity of the FE model. The accuracy of the FE analysis can be confirmed by comparing with the load-displacement (displacement is the average value of LVDT4 and LVDT 5) curves shown in Fig. 6 b).

As illustrated in Fig. 6 b), the curve of unreinforced specimen T-050 almost coincides with that of unreinforced specimen T-073 because the major deformation is contributed by the chord bending deflection, therefore the flexural stiffness becomes the dominant factor for the bearing capacity when β reaches 0.73. For T-025, before reaching 6%d_0, brittle crack had already occurred. However, the weld failure was not the typical failure modes of T-joints (i.e., chord plastification or punching shear) so the comparison between the maximum load caused by weld failure and the ultimate load of the other specimens is quite meaningless. Therefore, there was no ultimate load gained from the experiment. For T-025-R, T-050 and T-050-R, the ultimate loads of these specimens are determined by 6%d_0 deformation limit. Table 2 summarizes all the experimental ultimate strength results.

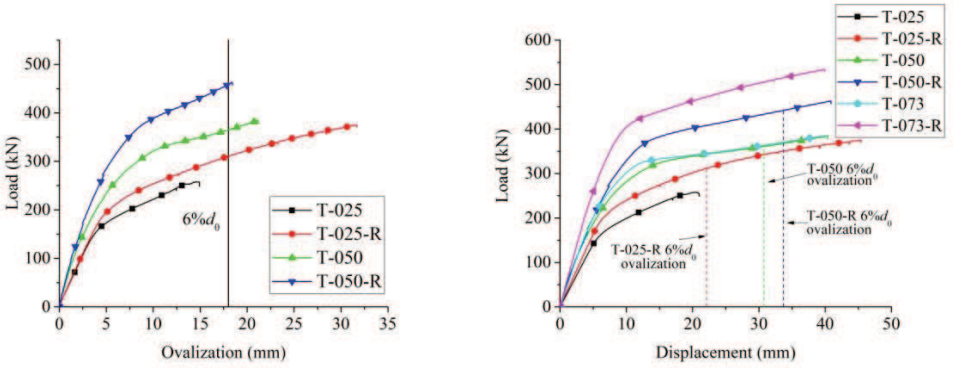

a) b)

Figure 6. Experimental curves: a) load-ovalization curves b) load-displacement curves

Table 2. Nominal strength and ultimate loads of experiment and FE analysis

Specimen	$F_{u,test}$ (kN)	$F_{u,A}$ (kN)	$F_{u,A}/F_{u,test}$	Strength increment (%)	
				Exp.	FE
T-025	-	277.8	-	-	-
T-025-R	311.2	316.9	1.02	-	14.1
T-050	367.4	363.8	0.99	-	-
T-050-R	458.9	465.2	1.01	24.9	27.9
T-073	-	381.9	-	-	-
T-073-R	-	505.5	-	-	32.4

Notes: $F_{u,test}$ = ultimate strength from test; $F_{u,A}$ = ultimate strength from numerical result.

4. FE modeling

FE software ANSYS 17.0 was adopted to establish FE models. The element SHELL181 was used to model the joints. The braces, chords, and stiffeners were assumed to obey the Von Mises yield criterion. The weld was assumed to be the elastic-perfect plastic material, meanwhile the weld fracture was not simulated in the numerical model. The yield stresses and the Young's modulus were obtained from material tests and the Poisson's ratio was set to 0.3 according to the Chinese design code (2003). The joint dimensions were defined according to the experimental specimens. The weld geometry was defined by the method shown in Zhu et al. (2014). The Y, Z displacements of each chord endplate were constrained meanwhile the X displacement of only one chord end was constrained in order to simulate the simply supported boundary condition. The axial tension applied to the brace endplate was replaced by displacement loading in the FE model. The large displacement was taken into account in static computation processes. Fig. 3 (right) illustrates deformation shapes of all specimens derived from FE analysis.

5. Comparison of results

The experimental and numerical load-ovalization curves for T-025 to T-050-R are presented in Fig. 7. As can be seen in the pictures, the numerical data are close to the experimental results both in elastic and elastic-plastic stages, with the ultimate strength difference less than 5%. For specimen T-025, no experimental ultimate strength is able to be used for comparison, but the difference between finite element and experimental results is within 10% after the ovalization reaches 5 mm.

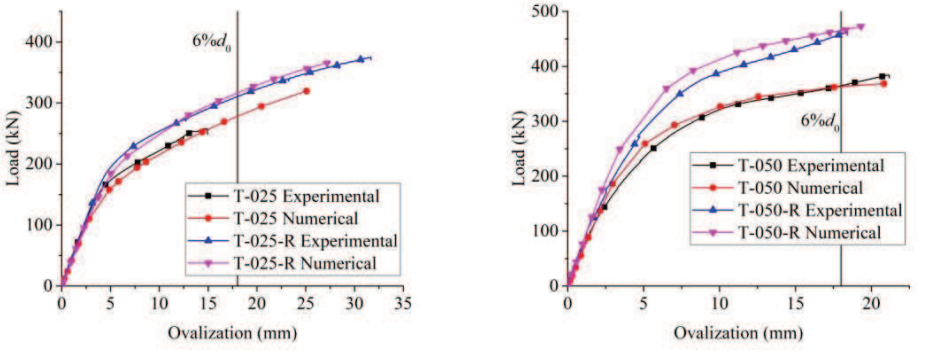

Figure 7. Comparison of experimental and numerical load-ovalization relationships

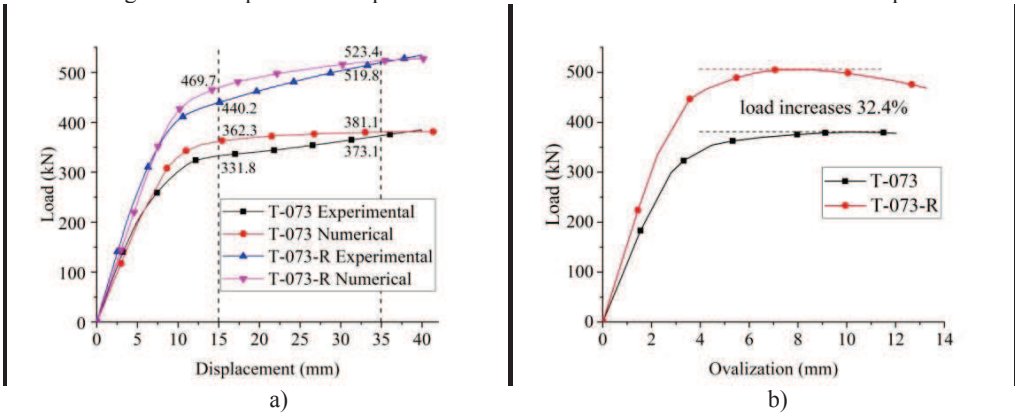

a) b)

Figure 8. Curves of T-073 and T-073-R: a) Comparison of experimental and numerical load-displacement relationships b) Numerical load-ovalization curves

Besides, the load-displacement curves for specimens T-073 and T-073-R are plotted in Fig. 8 a). By contrasting the FE and experimental figure when the displacements are 15 mm and 35 mm respectively, the validity of the FE analysis can be certified. The results of the comparison are shown in the picture, which shows that the differences between the experimental and FE analysis results are within 10%. Hence the FE analysis is accurate in reflecting the specimen's mechanical characteristics, and the load-ovalization curves obtained from the FE analysis are used to determine the ultimate strength of T-073 and T-073-R, as shown in Fig. 8 b).

As shown in Fig. 7 and Fig. 8 b), for T-025-R, the ultimate strength has increased by 14.1% compared with the referenced unreinforced specimen, and for specimen T-050-R, the enhancement is 27.9% (the result of the experiment is 24.9%). For specimens T-073 and T-073-R, the load-ovalization curves achieve their maximum values before the ovalizations reach 6% d_0, therefore the maximum loads represent the ultimate strength of joints T-073 and T-073-R, the difference between them is 32.4%. Meanwhile, the specimens' initial stiffness values are also increased by 3.3% for β of 0.25, 19.1% for β of 0.50, and 31.0% for β of 0.73.

Besides, the numerical load-ovalization curves of T-073 and T-073-R present obvious bending failure characteristics. For example, the FE analysis results showed a steady load stage that is the typical feature of bending failure of a simply supported beam. Hence, the chord finally fails due to the full plasticity of the crown section and thus the plastic moment $M_{\mathrm{pl},0}$ for T-073 can be determined as:

$$M_{pl,0} = \frac{1}{6} f_{y0} \left[d_0^3 - (d_0 - 2t_0)^3 \right] \tag{1}$$

Considering the effect of the brace diameter, the bending moment M at the crown point is $0.25F_1(l\text{-}d_1)$, in which F_1 is the load at the brace end (van der Vegte & Makino, 2005), l is the distance between two load points (2300mm). The value of the ultimate bend loading of T-073 calculated from the formula is 376 kN, which is consistent with the numerical results for T-073 (the numerical analysis result is 382kN). However, for T-073-R, the external stiffeners introduced an enhancement effect on the chord flexural capacity, and therefore the chord ultimate bend loading is much larger than that for T-073.

6. Conclusions

This study proves the following conclusions:

(i) The experimental results show that cracking occurred in the welding near the chord saddle position of the unreinforced specimen with β of 0.25. For the other specimens, the primary deformation was due to overall chord bending together with chord ovalization at mid-span. As a result, the failure mode for the specimens with β of 0.50 and the reinforced specimen with β of 0.25 was chord plastification. No joint failure appeared in the specimens with β of 0.73.

(ii) The results of experiment indicate that there is a significant enhancement in the bearing capacity of T-joints with external stiffeners compared with the unreinforced joints. Based on the experiment results and supplementary FE analysis, the ultimate strength increased by 14.1%, 24.9% and 32.4% for the specimens with β of 0.25, 0.50, and 0.73 respectively, while the initial stiffness increased by 3.3%, 19.1%, and 31.0% respectively. The effect of the external stiffeners was more evident with the β value increased. The ultimate strength of unreinforced specimens increased with the increase in β.

(iii) Satisfactory agreement was obtained between the numerical and experimental results of all specimens, not only for the initial stiffness but also for the elastic-plastic stage development, with the maximum differences less than 10%.

Acknowledgments

Supports from the Beijing Haiju Program, Beijing Advanced Innovation Center for Future Urban Design (Grant No. UDC2016030200), National Natural Science Foundation of China (No.51778035), the JiandaJieqing Plan and Beijing Cooperative Innovation Research Center on Energy Saving and Emission Reduction are gratefully acknowledged.

References

Ministry of Housing and Urban-Rural Construction of the People's Republic of China, *Code for design of steel structures*, China Planning Press, Beijing, 2003.

Choo, Y. S., van der Vegte, G. J., Zettlemoyer, N., Li, B. H., & Liew, J. Y. R., Static Strength of T-Joints Reinforced with Doubler or Collar Plates. I: Experimental Investigations. *Journal of Structural Engineering, 131*(1), 119-128, 2005.

van der Vegte, G. J., Choo, Y. S., Liang, J. X., Zettlemoyer, N., & Liew, J. Y. R., Static Strength of T-Joints Reinforced with Doubler or Collar Plates. II: Numerical Simulations. *Journal of Structural Engineering, 131*(1), 129-138, 2005.

Van der Vegte, G. J., & Makino, Y., Ultimate strength formulation for axially loaded CHS uniplanar T-joints. *In The Fifteenth International Offshore and Polar Engineering Conference.* International Society of Offshore and Polar Engineers, Jan, 2005.

Feng, Q., & Tan, J., Static strength of Y-joints reinforced with doubler plates under axial load. *China Offshore Platform*(05), 30-35, 2005.

Gao, Y., Liang, X., & Deng, X., *Metallic materials-Tensile testing-Method of test at ambient temperature*, China Quality and Standards Publishing Press, Beijing, 2010.

Sui, W., Chen, Y., Wang, Z., & Zhang, X., Study on tensile performance of doubler plate reinforced T-joints with circular chord and brace. *China Civ. Eng. J, 46*(5), 22-30, 2013.

Wang, F., Chen, Z., Liu, D., Luo, M., Ning, C., & Lan, X., Calculation method for bearing capacities of internal ring-stiffened tubular T- and Y-joints. *Journal of Southeast University (English Edition), 44*(4), 811-816, 2014.

Zhu, L., Zhao, Y., Li, S., Huang, Y., & Ban, L., Numerical analysis of the axial strength of CHS T-joints reinforced with external stiffeners. *Thin-Walled Structures, 85*, 481-488, 2014.

Luo, F. J., Yang, X., & Bai, Y., Member Capacity of Pultruded GFRP Tubular Profile with Bolted Sleeve Joints for Assembly of Latticed Structures. *Journal of Composites for Construction, 20*(3), 04015080, 2016.

Yang, X., Bai, Y., Luo, F. J., Zhao, X.-L., & Ding, F., Dynamic and fatigue performances of a large-scale space frame assembled using pultruded GFRP composites. *Composite Structures, 138*, 227-236, 2016.

Nassiraei, H., Lotfollahi-Yaghin, M. A., & Ahmadi, H., Static strength of offshore tubular T/Y-joints reinforced with collar plate subjected to tensile brace loading. *Thin-Walled Structures, 103*, 141-156, 2016. Yang, X., Bai, Y., Luo, F. J., Zhao, X.-L., & He, X.-h. (2017). Fiber-Reinforced Polymer Composite Members with Adhesive Bonded Sleeve Joints for Space Frame Structures. *Journal of Materials in Civil Engineering, 29*(2), 04016208. doi:10.1061/(asce)mt.1943-5533.0001737

Simões,. S. L., Simões, R., & Gervásio, H., Design of steel structures: Eurocode 3: Design of steel structures. S. l.: ECCS, European Convention for constructional steelwork, 2016.

Ding, Y., Zhu, L., Zhang, K., Bai, Y., & Sun, H., CHS X-joints strengthened by external stiffeners under brace axial tension. *Engineering Structures, 171*, 445-452, 2018.